THEORETICAL AND APPLIED MECHANICS
Volume 46 (2019) Issue 2, 157–171 DOI: https://doi.org/10.2298/TAM190228010W

TWO INTERACTING NON-ELLIPTICAL RIGID HARMONIC INCLUSIONS LOADED BY COUPLES

Xu Wang and Peter Schiavone

Abstract. We use conformal mapping techniques to design two interacting non-elliptical rigid inclusions, each of which is loaded by a couple, which ensure the so-called 'harmonic condition' in which the original mean stress in the matrix remains undisturbed after the introduction of the inclusions. We show that for prescribed Poisson's ratio and corresponding geometric parameters, several restrictions are necessary on the external loadings to ensure the harmonic condition. It is seen from our analysis that: (i) the interfacial and hoop stresses are uniformly distributed along each of the inclusion-matrix interfaces; (ii) the interfacial normal and hoop stresses along the two interfaces are completely determined by the Poisson's ratio and the constant mean stress in the matrix whilst the interfacial tangential stress along the two interfaces can be completely determined by the moments of the couples and the areas of the two inclusions; (iii) the existence of the applied couples will influence the non-elliptical shapes of the two rigid harmonic inclusions when the moment to area ratios for the two inclusions differ.

1. Introduction

When inhomogeneities (e.g. holes or inclusions) are introduced into an elastic material as part of the manufacture of composite structures, they inevitably lead to undesired stress concentrations which subsequently affect the intended mechanical performance of the structure. The design of *optimal* structural shapes of such inhomogeneities seeks to minimize or completely eliminate such stress concentrations. However, the identification of such shapes leads inevitably to an inverse problem in which we seek to determine the geometry of a boundary from prescribed conditions that must be satisfied by the final stress field. The approach used to solve such problems depends significantly on the pre-selected design criteria. The 'harmonic condition' advanced by Bjorkman and Richards [1, 2] and Richards and Bjorkman [3] is one such criterion which requires that the trace of the original stress field (or the original mean stress) in the surrounding matrix remains unchanged after the introduction of a hole or inclusion. In this case, the hole or inclusion

2010 *Mathematics Subject Classification:* 74B05; 74E30.
Key words and phrases: two rigid harmonic inclusions, couple, rigid-body rotation, constant interfacial and hoop stresses, conformal mapping.

is referred to as 'harmonic' (The terminology 'harmonic' is used in this context since the first invariant of the stress tensor is a harmonic function in linear plane elasticity.). In many situations, a harmonic shape will also satisfy the "constant strength" criterion proposed by Cherepanov [4] and will induce minimum stress concentration [5–7].

In previous discussions on the design of harmonic *rigid* inclusions, the inclusion is taken to be free of any external loading (see, for example, [3,5,6]). This, of course, is a simplification which limits the applicability of the corresponding mechanical model. Most recently, Wang and Schiavone [8] observed that it remains possible to satisfy the harmonic condition when a rigid elliptical inclusion is loaded by a couple. It is well-known, however, that, in general, considerable stress amplification will occur as a result of the interaction of *two* rigid inclusions placed relatively close together. Our research suggests that minimization of stress concentrations can still be realized for two interacting rigid *harmonic* inclusions when the inclusions are loaded externally by couples.

Accordingly, in this study, we examine the existence of two interacting non-elliptical rigid harmonic inclusions when each inclusion is loaded by a couple and the surrounding matrix is subjected to a uniform stress field at infinity. The design of the two rigid harmonic inclusions is achieved through the introduction of a conformal mapping function first adopted in Wang [9]. The presence of the couples means that the inclusions will undergo rigid-body rotations which can be determined via a moment balance for each inclusion. Once the harmonic condition is satisfied, the interfacial normal and tangential stresses and the hoop stress are found to be uniform along each one of the two inclusion-matrix interfaces.

2. Problem formulation

For plane deformations of a linearly isotropic elastic material, the stresses $(\sigma_{11}, \sigma_{22}, \sigma_{12})$, displacements (u_1, u_2) and stress functions (ϕ_1, ϕ_2) can be expressed in terms of two analytic functions $\varphi(z)$ and $\psi(z)$ of the complex variable $z = x_1 + \mathrm{i}x_2$ as [10, 11]

$$\sigma_{11} + \sigma_{22} = 2[\varphi'(z) + \overline{\varphi'(z)}], \quad \sigma_{22} - \sigma_{11} + 2\mathrm{i}\sigma_{12} = 2[\bar{z}\varphi''(z) + \psi'(z)],$$

$$2\mu(u_1 + \mathrm{i}u_2) = \kappa\varphi(z) - z\overline{\varphi'(z)} - \overline{\psi(z)}, \quad \phi_1 + \mathrm{i}\phi_2 = \mathrm{i}[\varphi(z) + z\overline{\varphi'(z)} + \overline{\psi(z)}],$$

where $\kappa = 3 - 4\nu$ for plane strain, $\kappa = (3-\nu)/(1+\nu)$ for plane stress and μ, $\nu (0 \leqslant \nu \leqslant 1/2)$ are the shear modulus and Poisson's ratio, respectively. In addition, the stresses are related to the stress functions through [11]

$$\sigma_{11} = -\phi_{1,2}, \quad \sigma_{12} = \phi_{1,1}, \quad \sigma_{21} = -\phi_{2,2}, \quad \sigma_{22} = \phi_{2,1}.$$

Let t_1 and t_2 be traction components along the x_1- and x_2-directions, respectively, on a given boundary L. If s is the arc-length measured along L such that the material remains on the left-hand side in the direction of increasing s, it can be shown that [11]

$$t_1 + \mathrm{i}t_2 = -\frac{d(\phi_1 + \mathrm{i}\phi_2)}{ds}. \tag{2.1}$$

Consider a domain in $\Re^2$, infinite in extent, containing two non-elliptical rigid inclusions. Let S denote the matrix, which is assumed to be perfectly bonded to the two inclusions through the left and right interfaces L_1 and L_2. The matrix is subjected to remote uniform in-plane stresses $(\sigma_{11}^{\infty}, \sigma_{22}^{\infty}, \sigma_{12}^{\infty})$ while the leftmost rigid inclusion with interface L_1 is loaded by a couple of moment M_1 and its right-hand counterpart with interface L_2 is loaded by a couple with moment M_2. In the following section, we will analyze, in detail, whether the two interacting non-elliptical rigid inclusions loaded by couples can indeed satisfy the harmonic condition.

3. Design of two interacting rigid harmonic inclusions loaded by couples

The boundary value problem in the physical z-plane takes the form

$$\begin{aligned} &\kappa\varphi(z) - z\overline{\varphi'(z)} - \overline{\psi(z)} = 2\mathrm{i}\mu\varpi_1 z, \quad z \in L_1; \\ &\kappa\varphi(z) - z\overline{\varphi'(z)} - \overline{\psi(z)} = 2\mathrm{i}\mu\varpi_2 z, \quad z \in L_2; \end{aligned} \tag{3.1}$$

$$\varphi(z) \cong \frac{\sigma_{11}^{\infty} + \sigma_{22}^{\infty}}{4} z + O(1), \quad \psi(z) \cong \frac{\sigma_{22}^{\infty} - \sigma_{11}^{\infty} + 2\mathrm{i}\sigma_{12}^{\infty}}{2} z + O(1), \quad |z| \to \infty, \tag{3.2}$$

where ϖ_1 and ϖ_2 re unknown rigid-body rotations of the left- and right- inclusions to be determined through moment equilibrium on each of the two inclusions. Equation (3.1) describes continuity of displacements across the two interfaces L_1 and L_2, respectively, whilst Eq. (3.2) gives the asymptotic behaviors of $\varphi(z)$ and $\psi(z)$ at infinity. In writing Eq. (3.1), we have disregarded the rigid-body translations of the two rigid inclusions.

Consider the following conformal mapping function for the matrix [9]

$$z = \omega(\xi) = R\left[\frac{1}{\xi - \lambda} + \frac{p}{\xi - \lambda^{-1}} + \frac{\Lambda^{-1} p}{\rho\xi - \lambda^{-1}} + \sum_{n=1}^{+\infty} \left(a_n \xi^n + a_{-n} \xi^{-n}\right)\right], \tag{3.3}$$

$$\xi(z) = \omega^{-1}(z), \quad 1 \leqslant |\xi| \leqslant \rho^{-\frac{1}{2}},$$

where R is a real scaling constant; λ $(1 < \lambda < \rho^{-1/2})$ is a real constant; p and Λ are complex constants and a_n, a_{-n} are unknown complex coefficients to be determined. Using the mapping function in Eq. (3.3), the matrix S in the z-plane is mapped onto an annulus $1 \leqslant |\xi| \leqslant \rho^{-1/2}$ in the ξ-plane, while the two interfaces L_1 and L_2 in the z-plane are mapped onto two co-axial circles with radii 1 and $\rho^{-1/2}$, respectively, in the ξ-plane. Furthermore, the point at infinity $(z = \infty)$ is mapped to the point $\xi = \lambda$.

In order to ensure that the two rigid inclusions are indeed harmonic, it is clear that $\varphi(z)$ should take the following form

$$\varphi(z) = Xz, \quad z \in S, \tag{3.4}$$

where X is a real constant.

By enforcing continuity of displacements across the two interfaces L_1 and L_2 in Eq. (3.1), we arrive at two expressions for $\psi(\xi) = \psi(\omega(\xi))(1 \leqslant |\xi| \leqslant \rho^{-1/2})$ as follows:

$$\psi(\xi) = R[X(\kappa-1)+2\mathrm{i}\mu\varpi_1]\left[\frac{1}{\xi^{-1}-\lambda}+\frac{\bar{p}}{\xi^{-1}-\lambda^{-1}} + \frac{\bar{\Lambda}^{-1}\bar{p}}{\rho\xi^{-1}-\lambda^{-1}}+\sum_{n=1}^{+\infty}\left(\bar{a}_n\xi^{-n}+\bar{a}_{-n}\xi^{n}\right)\right],$$

$$\psi(\xi) = R[X(\kappa-1)+2\mathrm{i}\mu\varpi_2]\left[\frac{1}{\rho^{-1}\xi^{-1}-\lambda}+\frac{\bar{p}}{\rho^{-1}\xi^{-1}-\lambda^{-1}} + \frac{\bar{\Lambda}^{-1}\bar{p}}{\xi^{-1}-\lambda^{-1}}+\sum_{n=1}^{+\infty}\left(\bar{a}_n\rho^{-n}\xi^{-n}+\bar{a}_{-n}\rho^{n}\xi^{n}\right)\right]. \tag{3.5}$$

In order to ensure that the elastic field in the matrix is unique, the above two expressions of $\psi(\xi)$ should coincide. As a result, we obtain

$$\Lambda = \frac{X(\kappa-1)-2\mathrm{i}\mu\varpi_2}{X(\kappa-1)-2\mathrm{i}\mu\varpi_1}, \tag{3.6}$$

and

$$a_n = \frac{\lambda^{-n-1}+p\Lambda^{-1}\rho^n\lambda^{n+1}}{1-\Lambda\rho^{-n}}, \quad a_{-n} = \frac{\lambda^{n-1}+p\lambda^{1-n}}{\Lambda^{-1}\rho^{-n}-1}, \quad n=1,2,\ldots,+\infty. \tag{3.7}$$

Imposing the asymptotic conditions in Eq. (3.2) on $\varpi(z)$ and $\psi(z)$, we obtain the following constraints

$$\begin{aligned} &\sigma_{11}^{\infty}+\sigma_{22}^{\infty}=4X,\\ &\sigma_{22}^{\infty}-\sigma_{11}^{\infty}+2\mathrm{i}\sigma_{12}^{\infty}=-2\bar{p}\lambda^2\left[X(\kappa-1)+2\mathrm{i}\mu\varpi_1\right]. \end{aligned} \tag{3.8}$$

From Eqs. (2.1), (3.4)–(3.5) and $(3.8)_1$, we deduce that the interfacial normal stress σ_{nn} and interfacial tangential stress σ_{nt}, are uniformly distributed along the two interfaces L_1 and L_2 as follows

$$\sigma_{nn} = X(\kappa+1) = \frac{(\kappa+1)(\sigma_{11}^{\infty}+\sigma_{22}^{\infty})}{4}, \quad \sigma_{nt} = -2\mu\varpi_1, \qquad z\in L_1; \tag{3.9}$$

$$\sigma_{nn} = X(\kappa+1) = \frac{(\kappa+1)(\sigma_{11}^{\infty}+\sigma_{22}^{\infty})}{4}, \quad \sigma_{nt} = -2\mu\varpi_2, \qquad z\in L_2. \tag{3.10}$$

It then follows from Eqs. (3.4), (3.9) and (3.10) that the hoop stress σ_{tt}, is also uniformly distributed along the two interfaces on the matrix side, specifically

$$\sigma_{tt} = X(3-\kappa) = \frac{(3-\kappa)(\sigma_{11}^{\infty}+\sigma_{22}^{\infty})}{4}, \quad z\in L_1\cup L_2.$$

The above expressions for σ_{nn} and σ_{tt}, which are completely determined by the Poisson's ratio and the constant mean stress in the matrix, are identical to the corresponding expressions obtained for a rigid harmonic elliptical inclusion in the absence of a couple [3] or in the presence of a couple applied to the rigid inclusion [8]. It is relatively straightforward to show that minimum stress concentration along the two interfaces has also been attained. In addition, moment equilibrium for

the left-hand inclusion enclosed by L_1 will yield expressions for σ_{nt} along the left interface L_1 and ϖ_1, in terms of the moment M_1 as follows

$$\sigma_{nt} = -\frac{M_1}{2A_1}, \quad \varpi_1 = \frac{M_1}{4\mu A_1}, \tag{3.11}$$

where A_1 is the area enclosed by L_1. A proof of Eq. (3.11) is given in the Appendix.

Similarly, moment equilibrium for the right-inclusion enclosed by L_2 will yield the following expressions for σ_{nt} along the right interface L_2 and ϖ_2 in terms of the moment M_2,

$$\sigma_{nt} = -\frac{M_2}{2A_2}, \quad \varpi_2 = \frac{M_2}{4\mu A_2}, \tag{3.12}$$

where A_2 is the area enclosed by L_2.

Using Eqs. $(3.8)_1$, (3.11) and (3.12), the complex number Λ in Eq. (3.6) can be further expressed in terms of the external loadings as

$$\Lambda = \frac{(\kappa-1)(\sigma_{11}^{\infty}+\sigma_{22}^{\infty}) - \frac{2\mathrm{i}M_2}{A_2}}{(\kappa-1)(\sigma_{11}^{\infty}+\sigma_{22}^{\infty}) - \frac{2\mathrm{i}M_1}{A_1}}, \tag{3.13}$$

which clearly indicates that Λ is loading dependent. Clearly the dependency of Λ in Eq. (3.13) on the areas A_1 and A_2 means that it is size-dependent.

It follows from Eqs. (3.8), (3.11) and (3.12) that the complex constant p can be uniquely determined as

$$p = \frac{\delta}{\lambda^2},$$

where δ is a complex loading parameter defined by

$$\delta = \frac{2(\sigma_{11}^{\infty} - \sigma_{22}^{\infty} + 2\mathrm{i}\sigma_{12}^{\infty})}{(\kappa-1)(\sigma_{11}^{\infty}+\sigma_{22}^{\infty}) - \frac{2\mathrm{i}M_1}{A_1}}. \tag{3.14}$$

Since δ in Eq. (3.14) depends on the area A_1, it is also size-dependent. Our previous results [9] indicate that $|\delta| \leqslant 1$. In the following, we will derive specific restrictions on the external loadings for given Poisson's ratio and geometric parameters $(R, \rho, \lambda, p, \Lambda)$ depending on whether Λ is real or complex.

Case 3.1. $\mathrm{Im}\{\Lambda\} \neq 0$

In this case, from Eqs. (3.13) and (3.14), we deduce that the loadings $(\sigma_{11}^{\infty}, \sigma_{22}^{\infty}, \sigma_{12}^{\infty}, M_1, M_2)$ are not independent and should satisfy the following restrictions:

$$\begin{aligned}
\frac{\sigma_{11}^{\infty} - \sigma_{22}^{\infty} + 2\mathrm{i}\sigma_{12}^{\infty}}{\sigma_{11}^{\infty}+\sigma_{22}^{\infty}} &= \frac{\mathrm{i}\delta(\kappa-1)(\bar{\Lambda}-1)}{2\Lambda''}, \\
\frac{\frac{M_1}{A_1}}{\sigma_{11}^{\infty}+\sigma_{22}^{\infty}} &= \frac{(1-\Lambda')(\kappa-1)}{2\Lambda''}, \\
\frac{\frac{M_2}{A_2}}{\sigma_{11}^{\infty}+\sigma_{22}^{\infty}} &= \frac{(\Lambda'-|\Lambda|^2)(\kappa-1)}{2\Lambda''},
\end{aligned} \tag{3.15}$$

where Λ' and $\Lambda''(\neq 0)$ are, respectively, the real and imaginary parts of Λ and $\delta = p\lambda^2$ is given.

CASE 3.2. $\mathrm{Im}\{\Lambda\} = 0$

When Λ is real-valued, from Eq. (3.13) we see that either $\sigma_{11}^{\infty} + \sigma_{22}^{\infty} = 0$ or $M_1/A_1 = M_2/A_2$.

(i) If $\sigma_{11}^{\infty} + \sigma_{22}^{\infty} = 0$, the external loadings should satisfy the following restrictions when $\delta \neq 0$

$$\begin{gathered} \sigma_{22}^{\infty} = -\sigma_{11}^{\infty}, \quad \delta'\sigma_{11}^{\infty} + \delta''\sigma_{12}^{\infty} = 0; \\ \frac{M_1}{A_1} = \frac{2(\delta''\sigma_{11}^{\infty} - \delta'\sigma_{12}^{\infty})}{|\delta|^2}, \\ \frac{M_2}{A_2} = \Lambda\frac{M_1}{A_1}, \end{gathered} \tag{3.16}$$

with δ and δ'' denoting, respectively, the real and imaginary parts of $\delta = p\lambda^2$. When $\delta = 0$ these loadings should satisfy the following restrictions

$$\begin{gathered} \sigma_{11}^{\infty} = \sigma_{22}^{\infty} = \sigma_{12}^{\infty} = 0, \\ \frac{M_2}{A_2} = \Lambda\frac{M_1}{A_1}, \end{gathered} \tag{3.17}$$

which clearly indicate the absence of the remote loading.

In the case of $\sigma_{11}^{\infty} + \sigma_{22}^{\infty} = 0$, both the interfacial normal and hoop stresses are zero along the two interfaces.

(ii) If $M_1/A_1 = M_2/A_2$, we have from Eq. (3.13) that $\Lambda = 1$. In this case, the external loadings should satisfy the following restrictions when $\delta \neq 0$

$$\begin{gathered} \left[|\delta|^2(\kappa-1) - 2\delta'\right]\sigma_{11}^{\infty} + \left[|\delta|^2(\kappa-1) + 2\delta'\right]\sigma_{22}^{\infty} - 4\delta''\sigma_{12}^{\infty} = 0, \\ \frac{M_1}{A_1} = \frac{\delta''(\sigma_{11}^{\infty} - \sigma_{22}^{\infty}) - 2\delta'\sigma_{12}^{\infty}}{|\delta|^2}, \\ \frac{M_2}{A_2} = \frac{M_1}{A_1}, \end{gathered} \tag{3.18}$$

and

$$\begin{gathered} \sigma_{11}^{\infty} = \sigma_{22}^{\infty} \neq 0, \quad \sigma_{12}^{\infty} = 0; \\ \frac{M_2}{A_2} = \frac{M_1}{A_1}, \end{gathered} \tag{3.19}$$

when $\delta = 0$ which indicates that the remote loading is hydrostatic or isotropic.

For given values of R, ρ, λ, p and Λ, the complex coefficients a_n, a_{-n} can be uniquely determined using Eq. (3.7). Thus the shapes of the two inclusions described by $z = \omega(\xi)$ for $|\xi| = 1$ and $\xi = \rho^{-1/2}$ are known completely which means that the areas A_1 and A_2 of the two inclusions can be readily determined. For a prescribed remote loading $(\sigma_{11}^{\infty}, \sigma_{22}^{\infty}, \sigma_{12}^{\infty})$ satisfying any of Eq. $(3.15)_1$, Eq. $(3.16)_1$, Eq. $(3.17)_1$, Eq. $(3.18)_1$ or Eq. $(3.19)_1$ and given (inclusion) areas, the two moments M_1 and M_2 (or the relationship between them) can then be determined, from Eqs. $(3.15)_{2,3}$, Eqs. $(3.16)_{2,3}$, Eq. $(3.17)_2$, Eqs. $(3.18)_{2,3}$ or Eq. $(3.19)_2$, respectively.

We note that $\Lambda \equiv 1$ always in the absence of the two couples ($M_1 = M_2 = 0$) (Wang, 2012). Thus, the presence of the couples most definitely influence the non-elliptical shapes of the two rigid harmonic inclusions when $\Lambda \neq 1$ or equivalently when $M_1/A_1 \neq M_2/A_2$. In other words, in the absence of any couple, all of the existing pairs of interacting non-elliptical rigid harmonic inclusions will cease to be harmonic when couples with dissimilar moment to area ratios are applied to the inclusions. For example, if the two moments have opposite signs, the moment to area ratios for the two inclusions will be unequal.

4. Discussion

In this section, we consider five special cases:

(i) $M_1 \neq 0,\ M_2 = 0$;
(ii) $M_1 = 0,\ M_2 \neq 0$;
(iii) $M_1/A_1 = -M_2/A_2$;
(iv) $\sigma_{11}^{\infty} + \sigma_{22}^{\infty} = 0,\ \delta' \neq 0,\ \delta'' = 0$;
(v) $M_1/A_1 = M_2/A_2,\ \delta' \neq 0,\ \delta'' = 0$.

4.1. $M_1 \neq 0,\ M_2 = 0$

In this case, we deduce from Eq. (3.15) that

$$\Lambda' - |\Lambda|^2 = 0, \tag{4.1}$$

and the external loadings should satisfy the following restrictions:

$$\begin{gathered} \frac{\sigma_{11}^{\infty} - \sigma_{22}^{\infty} + 2\mathrm{i}\sigma_{12}^{\infty}}{\sigma_{11}^{\infty} + \sigma_{22}^{\infty}} = \frac{\delta(\kappa - 1)}{2\Lambda}, \\ \frac{\frac{M_1}{A_1}}{\sigma_{11}^{\infty} + \sigma_{22}^{\infty}} = \frac{\Lambda''(\kappa - 1)}{2\Lambda'}. \end{gathered} \tag{4.2}$$

From Eqs. (3.11) and $(4.2)_2$, the interfacial tangential stress σ_{nt} along the left interface L_1 and the rigid-body rotation of the left-inclusion ϖ_1 can be expressed in terms of the remote loading as

$$\sigma_{nt} = -\frac{\Lambda''(\kappa - 1)(\sigma_{11}^{\infty} + \sigma_{22}^{\infty})}{4\Lambda'}, \quad \varpi_1 = \frac{\Lambda''(\kappa - 1)(\sigma_{11}^{\infty} + \sigma_{22}^{\infty})}{8\mu\Lambda'}.$$

From Eq. (3.12) it now follows that the interfacial tangential stress σ_{nt} along the right interface L_2 and the rigid-body rotation of the right-inclusion ϖ_2 are both zero.

For example, the harmonic shapes of the two rigid inclusions are illustrated in Fig. 1 when $\rho = 0.1$, $\lambda = \rho^{-\frac{1}{4}} = 1.7783$, $p = 0$ and $\Lambda = \frac{1}{2}(1 - \mathrm{i})$ in Eq. (4.1).

4.2. $M_1 = 0,\ M_2 \neq 0$

In this case, from Eq. (3.15) we deduce that

$$\Lambda' = 1, \tag{4.3}$$

and the external loadings should satisfy the following restrictions:

$$\begin{aligned} \frac{\sigma_{11}^{\infty}-\sigma_{22}^{\infty}+2\mathrm{i}\sigma_{12}^{\infty}}{\sigma_{11}^{\infty}+\sigma_{22}^{\infty}} &= \frac{\delta(\kappa-1)}{2}, \\ \frac{\frac{M_2}{A_2}}{\sigma_{11}^{\infty}+\sigma_{22}^{\infty}} &= -\frac{\Lambda''(\kappa-1)}{2}. \end{aligned} \tag{4.4}$$

From Eq. (3.11) we see that the interfacial tangential stress σ_{nt} along the left interface L_1 and the rigid-body rotation of the left-inclusion ϖ_1 are now both zero.

Eqs. (3.12) and $(4.4)_2$ determine that the interfacial tangential stress σ_{nt} along the right interface L_2 and the rigid-body rotation of the right-inclusion ϖ_2 can be expressed in terms of the remote loading as

$$\sigma_{nt}=\frac{\Lambda''(\kappa-1)(\sigma_{11}^{\infty}+\sigma_{22}^{\infty})}{4}, \quad \varpi_2=-\frac{\Lambda''(\kappa-1)(\sigma_{11}^{\infty}+\sigma_{22}^{\infty})}{8\mu}.$$

For example, the harmonic shapes of the two rigid inclusions are shown in Fig. 2 in the case $\rho=0.1$, $\lambda=\rho^{-\frac{1}{4}}=1.7783$, $p=0$ and $\Lambda=1+2.11\mathrm{i}$ in Eq. (4.3). It is interesting to note in Fig. 2 the emergence of a non-smooth boundary, specifically the appearance of a sharp corner on the boundary of the left rigid inclusion which is here free of the effects of the couple.

4.3. $M_1/A_1=-M_2/A_2$

In this case, from Eq. (3.15) we deduce that

$$|\Lambda|=1, \tag{4.5}$$

and the external loadings should satisfy the following restrictions:

$$\begin{aligned} \frac{\sigma_{11}^{\infty}-\sigma_{22}^{\infty}+2\mathrm{i}\sigma_{12}^{\infty}}{\sigma_{11}^{\infty}+\sigma_{22}^{\infty}} &= \frac{\mathrm{i}\delta(\kappa-1)(\bar{\Lambda}-1)}{2\Lambda''}, \\ \frac{\frac{M_1}{A_1}}{\sigma_{11}^{\infty}+\sigma_{22}^{\infty}} &= -\frac{\frac{M_2}{A_2}}{\sigma_{11}^{\infty}+\sigma_{22}^{\infty}}=\frac{(1-\Lambda')(\kappa-1)}{2\Lambda''}. \end{aligned} \tag{4.6}$$

From Eqs. (3.11) and $(4.6)_2$ the interfacial tangential stress σ_{nt} along the left interface L_1 and the rigid-body rotation of the left-inclusion ϖ_1 can be expressed in terms of the remote loading as

$$\sigma_{nt}=-\frac{(1-\Lambda')(\kappa-1)(\sigma_{11}^{\infty}+\sigma_{22}^{\infty})}{4\Lambda''}, \quad \varpi_1=\frac{(1-\Lambda')(\kappa-1)(\sigma_{11}^{\infty}+\sigma_{22}^{\infty})}{8\mu\Lambda''}.$$

Eqs. (3.12) and $(4.6)_2$ now give us that the interfacial tangential stress σ_{nt} along the right interface L_2 and the rigid-body rotation of the right-inclusion ϖ_2 can be expressed in terms of the remote loading as

$$\sigma_{nt}=\frac{(1-\Lambda')(\kappa-1)(\sigma_{11}^{\infty}+\sigma_{22}^{\infty})}{4\Lambda''}, \quad \varpi_2=-\varpi_1=-\frac{(1-\Lambda')(\kappa-1)(\sigma_{11}^{\infty}+\sigma_{22}^{\infty})}{8\mu\Lambda''}.$$

For example, the harmonic shapes of the two rigid inclusions are shown in Fig. 3 when $\rho=0.1$, $\lambda=\rho^{-\frac{1}{4}}=1.7783$, $p=0$ and $\Lambda=\exp(\frac{\pi}{6}\mathrm{i})$ in Eq. (4.5). We can see from Fig. 3 that $A_1=A_2$ due to the fact that the two inclusions have identical shapes and sizes. As a result, we will have $M_1=-M_2$.

4.4. $\sigma_{11}^{\infty}+\sigma_{22}^{\infty}=0$, $\delta'\neq 0$, $\delta''=0$

In this case, Eq. (3.16) reduces to

$$\sigma_{11}^{\infty}=\sigma_{22}^{\infty}=0, \quad \frac{M_1}{A_1}=-\frac{2\sigma_{12}^{\infty}}{\delta'}, \quad \frac{M_2}{A_2}=-\frac{2\Lambda\sigma_{12}^{\infty}}{\delta'}.$$

The tangential stress along the left interface L_1 and the rigid-body rotation of the left-inclusion can be expressed in terms of the remote shear stress as

$$\sigma_{nt}=\frac{\sigma_{12}^{\infty}}{\delta'}, \quad \varpi_1=-\frac{\sigma_{12}^{\infty}}{2\mu\delta'}. \tag{4.7}$$

The tangential stress along the right interface L_2 and the rigid-body rotation of the right inclusion can be expressed in terms of the remote shear stress as

$$\sigma_{nt}=\frac{\Lambda\sigma_{12}^{\infty}}{\delta'}, \quad \varpi_2=-\frac{\Lambda\sigma_{12}^{\infty}}{2\mu\delta'}. \tag{4.8}$$

It is further deduced from Eqs. (4.7) and (4.8) that $|\sigma_{nt}\geqslant|\sigma_{12}^{\infty}|$ along L_1 and $|\sigma_{nt}|\geqslant|\Lambda\sigma_{12}^{\infty}|$ along L_2 in view of the fact that $|\delta|\leqslant 1$, Recall that in this case, the interfacial normal and hoop stresses along the two interfaces are zero.

For example, in the case $\rho=0.1$, $\lambda=\rho^{-\frac{1}{4}}=1.7783$, $p=-0.1$ and $\Lambda=2$, the harmonic shapes of the two rigid inclusions are shown in Fig. 4. In this example, we have $\delta=-0.3162$. We again note the emergence of non-smooth boundaries in the extreme cases depicted in Figures 5 and 6. In fact, in Fig. 5 we present the harmonic shapes of the two rigid inclusions when $\rho=0.1$, $\lambda=\rho^{-\frac{1}{4}}=1.7783$, $p=-0.1$ and $\Lambda=3.39$ with $\delta=-0.3162$ and, in Fig. 6, the harmonic shapes when $\rho=0.1$, $\lambda=\rho^{-\frac{1}{4}}=1.7783$, $p=-0.112$ and $\Lambda=0.28$ with $\delta=-0.3542$. We can see from Fig. 5 that two sharp corners appear on the boundary of the left rigid inclusion while in Fig. 6 as many as three sharp corners may emerge on the boundary of the right rigid inclusion.

4.5. $M_1/A_1=M_2/A_2$, $\delta'\neq 0$, $\delta''=0$

In this case, Eq. (3.18) reduces to

$$\begin{gathered}[\delta'(\kappa-1)-2]\,\sigma_{11}^{\infty}+[\delta'(\kappa-1)+2]\,\sigma_{22}^{\infty}=0,\\ \frac{M_1}{A_1}=\frac{M_2}{A_2}=-\frac{2\sigma_{12}^{\infty}}{\delta'}.\end{gathered} \tag{4.9}$$

The tangential stress along the two interfaces and the rigid-body rotations of the two inclusions can be expressed in terms of the remote shear stress as

$$\sigma_{nt}=\frac{\sigma_{12}^{\infty}}{\delta'} \quad (z\in L_1\cup L_2), \qquad \varpi_1=\varpi_2=-\frac{\sigma_{12}^{\infty}}{2\mu\delta'}. \tag{4.10}$$

It is further deduced from Eq. (4.10) that $|\sigma_{nt}|\geqslant|\sigma_{12}^{\infty}|$ along L_1 and L_2 in view of the fact that $|\delta|\leqslant 1$. In this case, by considering Eq. (4.9) and the fact that $\Lambda\equiv 1$, the two couples will exert no influence on the shapes of the two inclusions. Furthermore, if we choose $\lambda=\rho^{-\frac{1}{4}}$, the shapes and sizes of the two inclusions are identical [9]. As a result, we will have $A_1=A_2$ and $M_1=M_2$.

For example, the identical harmonic shapes of the two rigid inclusions are shown in Fig. 7 when $\rho=0.1$, $\lambda=\rho^{-\frac{1}{4}}=1.7783$, $p=-0.1$, $\Lambda=1$ with $\delta=-0.3162$.

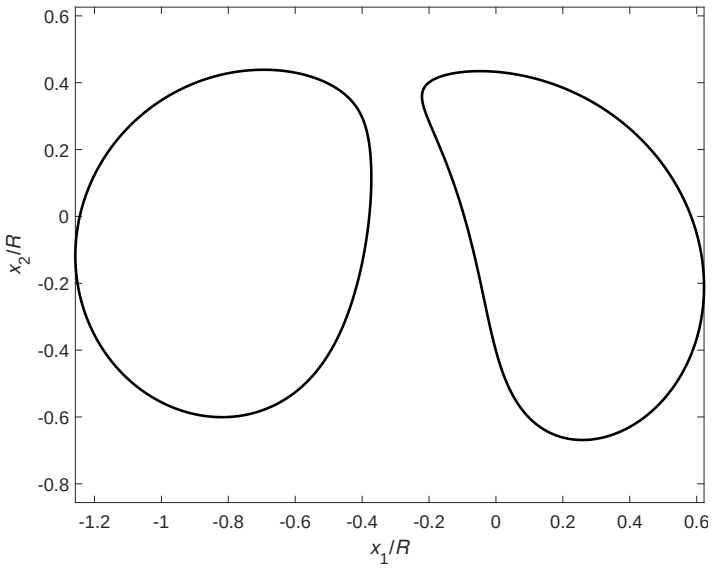

FIGURE 1. The harmonic shapes of the two rigid inclusions when choosing $\rho = 0.1$, $\lambda = \rho^{-\frac{1}{4}} = 1.7783$, $p = 0$ and $\Lambda = \frac{1}{2}(1 - \mathrm{i})$.

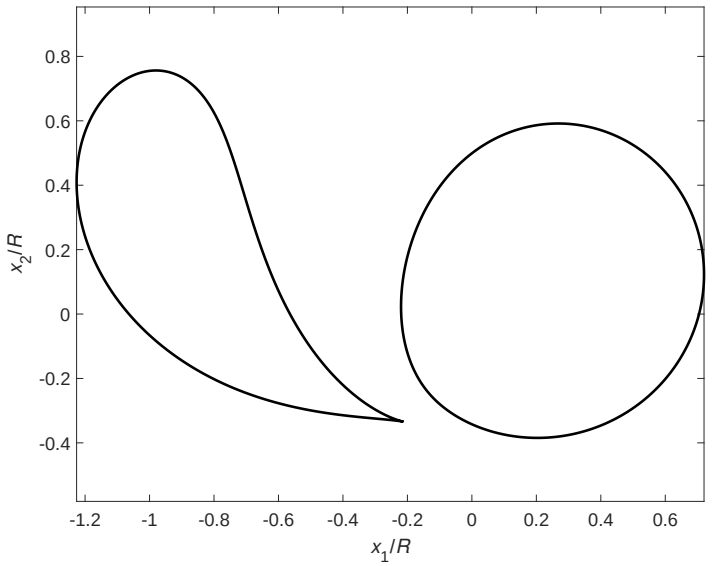

FIGURE 2. The harmonic shapes of the two rigid inclusions when choosing $\rho = 0.1$, $\lambda = \rho^{-\frac{1}{4}} = 1.7783$, $p = 0$ and $\Lambda = 1 + 2.11\mathrm{i}$. A sharp corner exists on the boundary of the left rigid inclusion free of couple.

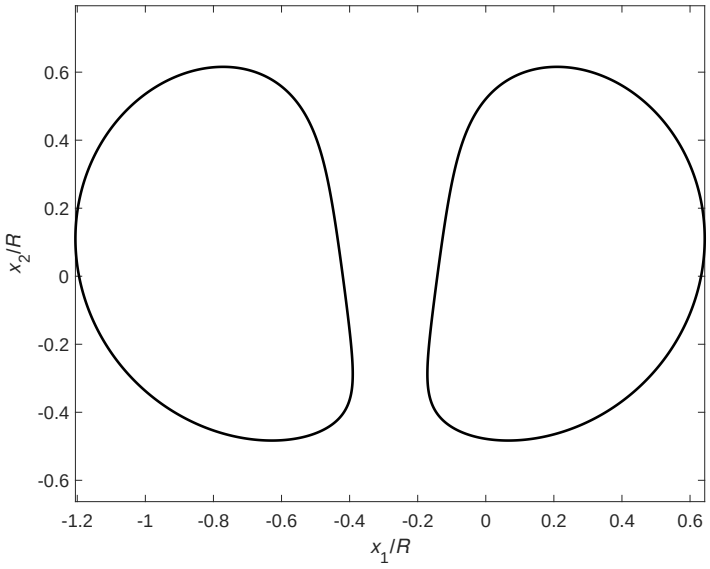

FIGURE 3. The identical harmonic shapes of the two rigid inclusions when choosing $\rho = 0.1$, $\lambda = \rho^{-\frac{1}{4}} = 1.7783$, $p = 0$ and $\Lambda = \exp(\frac{\pi}{6}\mathrm{i})$.

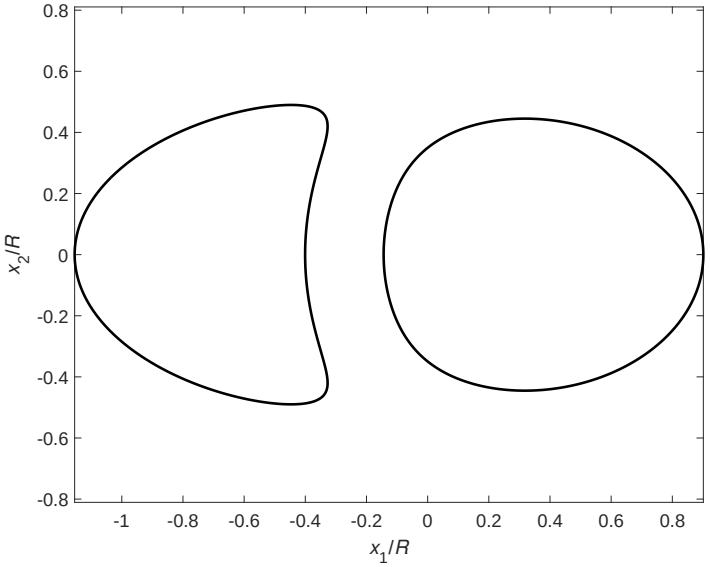

FIGURE 4. The harmonic shapes of the two rigid inclusions when choosing $\rho = 0.1$, $\lambda = \rho^{-\frac{1}{4}} = 1.7783$, $p = -0.1$ and $\Lambda = 2$.

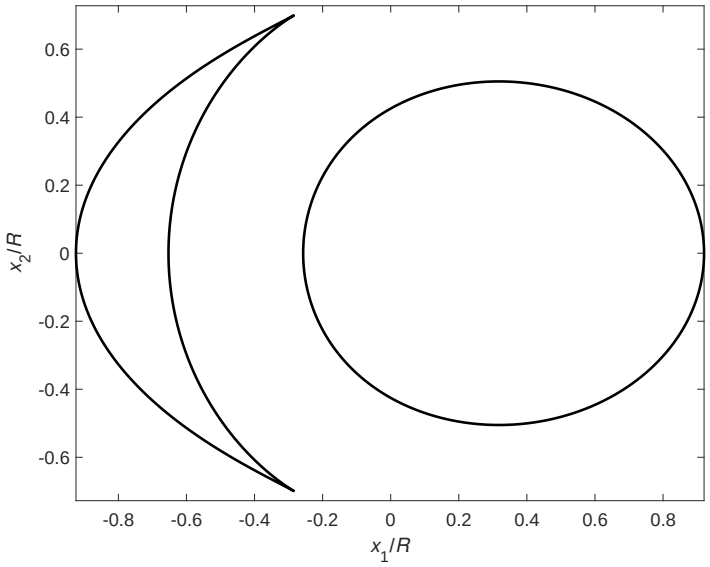

FIGURE 5. The harmonic shapes of the two rigid inclusions when choosing $\rho = 0.1$, $\lambda = \rho^{-\frac{1}{4}} = 1.7783$, $p = -0.1$ and $\Lambda = 3.39$. Two sharp corners exist on the boundary of the left rigid inclusion.

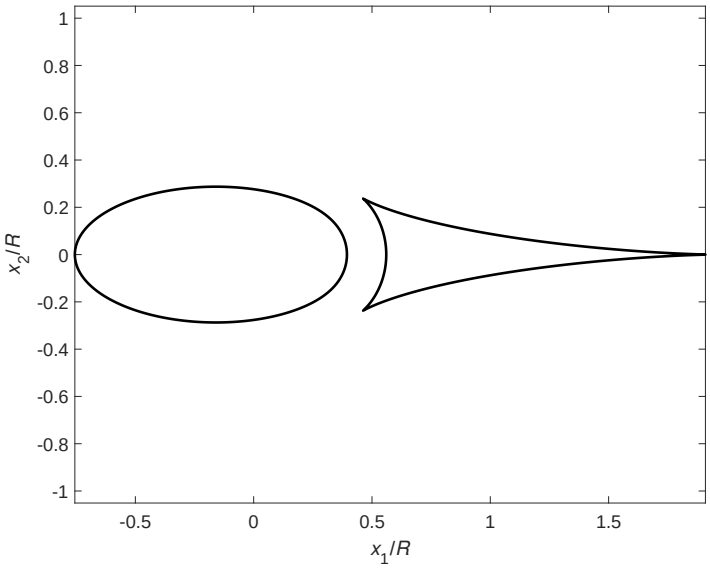

FIGURE 6. The harmonic shapes of the two rigid inclusions when choosing $\rho = 0.1$, $\lambda = \rho^{-\frac{1}{4}} = 1.7783$, $p = -0.112$ and $\Lambda = 0.28$. Three sharp corners exist on the boundary of the right rigid inclusion.

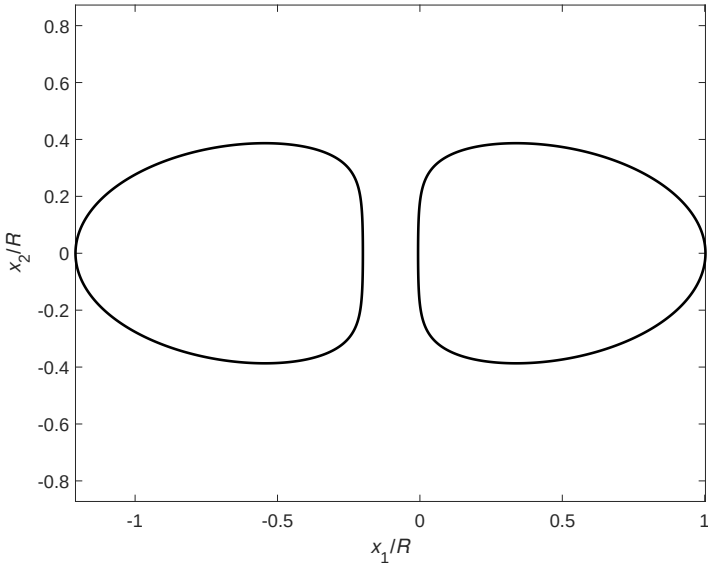

FIGURE 7. The identical harmonic shapes of the two rigid inclusions when choosing $\rho = 0.1$, $\lambda = \rho^{-\frac{1}{4}} = 1.7783$, $p = -0.1$ and $\Lambda = 1$.

We emphasize that the harmonic shapes in Figures 1 to 6 cannot be observed when the couples are absent. Only the harmonic shapes in Fig. 7 can be observed in the absence of couples.

5. Conclusions

We present a solution to the inverse problem concerned with the design of two interacting rigid harmonic inclusions, each of which is loaded by a couple. Our analysis shows that once the four parameters ρ, λ, p and Λ are given, all of the complex coefficients appearing in the mapping function can be uniquely determined. In order to ensure that the harmonic condition is satisfied, several restrictions on the loadings are obtained and described in: Eq. (3.15) when $\Lambda'' \neq 0$; Eq. (3.16) when $\sigma_{11}^{\infty} + \sigma_{22}^{\infty} = 0$ and $\delta \neq 0$; Eq. (3.17) when $\sigma_{11}^{\infty} + \sigma_{22}^{\infty} = 0$ and $\delta = 0$; Eq. (3.18) when $M_1/A_1 = M_2/A_2$ and $\delta \neq 0$; Eq. (3.19) when $M_1/A_1 = M_2/A_2$ and $\delta = 0$. Once these restrictions are met, the interfacial normal and tangential stresses and the hoop stress are uniformly distributed along each one of two interfaces L_1 and L_2.

Appendix A.

Moment equilibrium on the left-inclusion can be expressed as

$$M_1 = \oint_{L_1} (t_1 x_2 - t_2 x_1) \mathrm{d}s = -\operatorname{Im}\left\{ \oint_{L_1} (t_1 + \mathrm{i}t_2)\bar{z}\mathrm{d}s \right\}$$

$$
\begin{aligned}
(\text{A.1}) \qquad &= -\operatorname{Im}\left\{\oint_{L_1}(\sigma_{nn}+\mathrm{i}\sigma_{nt})\mathrm{e}^{\mathrm{i}n(z)}\bar{z}\mathrm{d}s\right\} = \operatorname{Re}\left\{\oint_{L_1}(\sigma_{nn}+\mathrm{i}\sigma_{nt})\bar{z}\mathrm{d}z\right\} \\
&= \sigma_{nn}\oint_{L_1}(x_1\mathrm{d}x_1+x_2\mathrm{d}x_2)-\sigma_{nt}\oint_{L_1}(x_1\mathrm{d}x_2-x_2\mathrm{d}x_1) \\
&= -2\sigma_{nt}\iint_{S_1}\mathrm{d}x_1\mathrm{d}x_2 = -2\sigma_{nt}A_1,
\end{aligned}
$$

where the line integral is taken in the counterclockwise direction, $\mathrm{e}^{\mathrm{i}n(z)}$ represents (in complex form) the outward normal to L_1 at z and S_1 is the region enclosed by L_1. Note that both σ_{nn} and σ_{nt} are constant along the interface L_1. In deriving Eq. (A.1), Green's theorem has been applied to convert the line integral to a double integral.

From the above we have that

$$\sigma_{nt} = -\frac{M_1}{2A_1}, \quad z \in L_1.$$

In view of this expression for σ_{nt} and the corresponding expression for σ_{nt} in Eq. (3.9), we arrive at

$$\varpi_1 = \frac{M_1}{4\mu A_1}.$$

This proves Eq. (3.11).

Acknowledgements. This work is supported by the National Natural Science Foundation of China (Grant No. 11272121) and through a Discovery Grant from the Natural Sciences and Engineering Research Council of Canada (Grant No: RGPIN-2017-03716115).

References

1. G. S. Bjorkman, R. Richards, *Harmonic holes–an inverse problem in elasticity*, ASME J. Appl. Mech. **43** (1976), 414–418.
2. G. S. Bjorkman, R. Richards, *Harmonic holes for nonconstant fields*, ASME J. Appl. Mech. **46** (1979), 573–576.
3. R. Richards, G. S. Bjorkman, *Harmonic shapes and optimum design*, J. Eng. Mech. Div., Proc. ASCE **106** (1980), 1125–1134.
4. G. P. Cherepanov, *Inverse problems of the plane theory of elasticity*, Prikl. Mat. Mekh. **38** (1974), 963–979.
5. L. T. Wheeler, *The problem of minimizing stress concentration at a rigid inclusion*, ASME J. Appl. Mech. **52** (1985), 83–86.
6. L. T. Wheeler, *Stress minimum forms for elastic solids*, Appl. Mech. Rev. **45** (1992), 1–11.
7. C. Q. Ru, *Three-phase elliptical inclusions with internal uniform hydrostatic stresses*, J. Mech. Phys. Solids **47** (1999), 259–273.
8. X. Wang, P. Schiavone, *A coated rigid elliptical inclusion loaded by a couple in the presence of uniform interfacial and hoop stresses*, Comptes Rendus Mécanique **346** (2018), 477–481.
9. X. Wang, *Uniform fields inside two non-elliptical inclusions*, Math. Mech. Solids **17** (2012), 736–761.
10. N. I. Muskhelishvili, *Some Basic Problems of the Mathematical Theory of Elasticity*, P. Noordhoff Ltd., Groningen, 1953.
11. T. C. T. Ting, *Anisotropic Elasticity-Theory and Applications*, Oxford University Press, New York, 1996.

ДВЕ ИНТЕРАГУЈУЋЕ НЕ-ЕЛИПТИЧКЕ КРУТЕ ХАРМОНИЧКЕ ИНКЛУЗИЈЕ ИСПУЊЕНЕ ПАРОВИМА

Резиме. У раду се користе технике конформналних пресликавања ради дизајнирања две интереагујуће не-елиптичне круте инклузије, од којих је свака испуњено од стране пара, који обезбеђује такозвано 'хармонично стање' у коме почетни средњи напон у матрици остаје непромењен након увођења инклузије.

Показујемо да је за унапред прописан Пуасонов однос и геометријске параметре потребно неколико ограничења на спољашња оптерећења како би се осигурало хармонично стање. Из наше анализе се види да: (i) интерфејсни и обручни напони су равномерно распоређени дуж сваке инклузија-матрице интерфејса; (ii) интерфејсни нормални и напони обруча дуж два интерфејса у потпуности се одређују Пуасоновим односом и константним средњим напоном у матрици, док се међуфазни тангенцијални напон дуж два интерфејса у потпуности може одредити моментима парова и подручја две инклузије; (iii) постојање примењених парова ће утицати на не-елиптичне облике две круте хармоничке инклузије када се односи момента и површине за две инклузије разликују.

School of Mechanical and Power Engineering
East China University of Science and Technology
Shanghai
China
xuwang@ecust.edu.cn

Department of Mechanical Engineering
University of Alberta
10-203 Donadeo Innovation Centre for Engineering Edmonton
Alberta
Canada
p.schiavone@ualberta.ca

(Received 28.02.2019.)
(Available online 21.11.2019.)